Cascaded observers to improve lateral vehicle state and tyre parameter estimates

Robert Daily, William Travis
and David M. Bevly*

Department of Mechanical Engineering,
GPS and Vehicle Dynamics Lab,
Auburn University, AL 36849, USA
E-mail: dailyrl@auburn.edu E-mail: traviwe@auburn.edu
E-mail: bevlydm@auburn.edu
*Corresponding author

Abstract: This paper proposes a method to produce high update, accurate, observable estimates of vehicle sideslip, utilising a two antenna GPS system. Measurements are blended with a kinematic Kalman filter to get high update sideslip estimates, which are used to predict the Dugoff tyre parameters. The parameters are then used in a model-based Kalman filter, which can provide more accurate vehicle state estimates even in the event of a GPS outage. Tyre force estimation is tested with experimental data on high and low friction surfaces, and validated by the performance of the model-based Kalman filter using the identified tyre parameters.

Keywords: vehicle dynamics; sideslip; dual antenna GPS; Kalman filter; estimation; kinematic model.

Reference to this paper should be made as follows: Daily, R., Travis, W. and Bevly, D.M. (xxxx) 'Cascaded observers to improve lateral vehicle state and tyre parameter estimates', *Int. J. Vehicle Autonomous Systems*, Vol. x, No. x, pp.xxx–xxx.

Biographical notes: Robert Daily is a PhD candidate in Mechanical Engineering at Auburn University. He graduated from Auburn with his MS in ME in 2005 and his BS in ME in 2000. He works in the GPS and Vehicle Dynamics Lab studying control and path planning of autonomous ground vehicles.

William Travis is pursuing a MS in Mechanical Engineering from Auburn University. He graduated from Auburn with a BS in ME in 2004. He works in the GPS and Vehicle Dynamics Lab studying navigation for ground vehicles.

David M. Bevly is an Assistant Professor at Auburn University and head of the GPS and Vehicle Dynamics Lab. He received his PhD in Mechanical Engineering from Stanford University in 2001, his MS in ME from Massachusetts Institute of Technology in 1997, and his BS in ME from Texas A&M University in 1995.

1 Introduction

Sideslip estimation is a critical aspect of many Electronic Stability Control (ESC) systems (Tseng et al., 1999; Hac and Simpson, 2000; Nishio et al., 2001; van Zanten, 2002). Sideslip estimation schemes fall into two categories, model-based and kinematic. Model-based estimators use a dynamic lateral vehicle model such as the bicycle model (Farrelly and Wellstead, 1996), while kinematic estimators use the kinematic relationships between the measurements of different sensors such as GPS and Inertial Measurement Units (IMU) (Bevly et al., 2002, O'Brien, 2006). Model based estimators are typically cleaner than kinematic estimators; however, they require knowledge about the vehicle parameters that is often difficult to obtain (such as cornering stiffnesses). The only vehicle dependent knowledge kinematic estimators require is the location of the sensors and CG to translate velocities and accelerations to a common point; even this is often neglected.

Previous research has begun to combine the methods by predicting the tyre cornering stiffness for the linear region of the tyre (Bevly et al., 2001; Anderson and Bevly, 2004). This work presents a method to combine the best aspects of kinematic and model-based estimators in a cascaded approach and extends the estimation of states and parameters into the non-linear region of the tyre. First, a kinematic estimator is used to determine initial estimates of the states. These estimates are used to predict the cornering stiffness and peak lateral force of the front and rear axles by estimating the lateral force and tyre slip angle over the entire operating range. Finally, using these (and other) vehicle parameters, a model-based estimator is used to get clean estimates of the vehicle states, sideslip in particular. These estimates are reliable during GPS outages, which would be beneficial to ESC systems on vehicle operating in GPS denied areas, such as urban canyons or on heavily wooded roads. Along with the sideslip estimate, the tyre information (cornering stiffness and peak lateral force) could be used to improve ESC systems, especially in situations where road conditions vary.

To validate this research, the algorithms are tested on an Infiniti G35 outfitted with a data acquisition system measuring among other things steer angle, lateral acceleration, yaw rate, and GPS position and velocity. A dual antenna GPS system mounted on the vehicle measures true roll angle and heading. A Datron^{TM} optical velocity sensor provides a direct measurement of sideslip that is compared to the GPS sideslip measurement. Experiments are performed on low and high coefficient of friction surfaces (gravel and dry asphalt) generating excessive sideslip to analyse the tyre parameter estimation method and the performance of the model-based Kalman filter in the non-linear handling region. The importance of GPS based sideslip measurements and tyre parameter estimation is also shown in this paper.

2 Vehicle model

Figure 1 shows a simple schematic of a vehicle known as the bicycle model. The model neglects weight transfer from inner to outer tyres and assumes the same tyres and slip angles on the inner and outer wheels (Gillespie, 1992).

Figure 1 Bicycle model

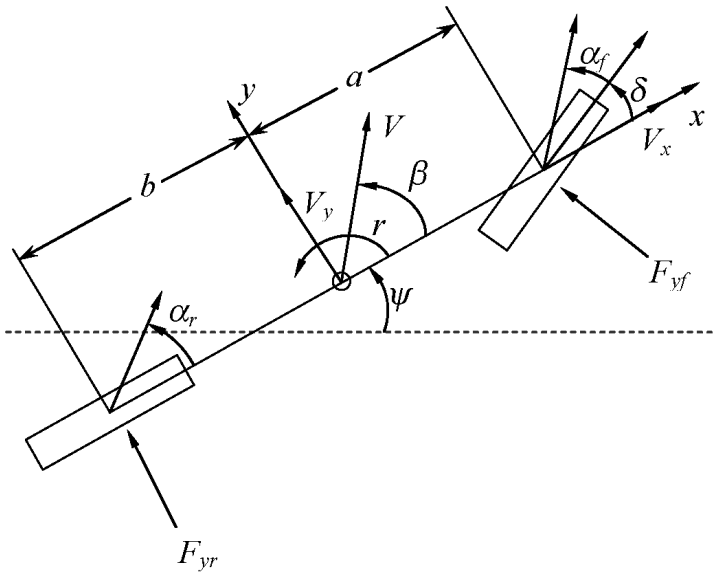

Solving for sideslip rate $(\dot{\beta})$ and yaw acceleration $(\dot{r})$ yields

$$\begin{aligned}\dot{\beta} &= \frac{2F_{yf}\cos(\delta) + 2F_{yr} + mg\sin(\theta_{\text{bank}})}{mV_x} - r \\ \dot{r} &= \frac{2aF_{yf}\cos(\delta) - 2bF_{yr}}{I_z}.\end{aligned} \tag{1}$$

Utilising a linear tyre model and assuming small angles and no bank angle, these equations can be written in state space form:

$$\begin{bmatrix}\dot{\beta} \\ \dot{r}\end{bmatrix} = \begin{bmatrix}(-C_{\alpha f} - C_{\alpha r})/(mV) & (-aC_{\alpha f} + bC_{\alpha r})/(mV^2) - 1 \\ (-aC_{\alpha f} + bC_{\alpha r})/(I_z) & (-a^2C_{\alpha f} - b^2C_{\alpha r})/(I_zV)\end{bmatrix}\begin{bmatrix}\beta \\ r\end{bmatrix} + \begin{bmatrix}C_{af}/mV \\ aC_{\alpha f}/I_z\end{bmatrix}\delta. \tag{2}$$

For steady state cornering, the understeer gradient is defined as

$$K_{US} = \frac{m}{L}\left(\frac{bC_{\alpha r} - aC_{\alpha f}}{C_{\alpha f}C_{\alpha r}}\right). \tag{3}$$

In a neutral steer vehicle the understeer gradient is zero; the state transition matrix from equation (2) simplifies to

$$\mathbf{A} = \begin{bmatrix}(-C_{\alpha f} - C_{\alpha r})/mV & -1 \\ 0 & (-a^2C_{\alpha f} - b^2C_{\alpha r})/I_zV\end{bmatrix}. \tag{4}$$

Note this allows yaw rate to be independent of sideslip, but sideslip is still dependent upon yaw rate. This results in the sideslip being unobservable with only a yaw rate measurement.

To allow the model to capture a wider range of vehicle behaviour a more complicated tyre model may be used. The Dugoff tyre model is a good choice for its ability to approximate the tyre curve with physical parameters: lateral tyre stiffness (C_α) and peak friction coefficient (μ) (Dugoff et al., 1970). The inputs into the model are tyre slip angle (α), and vertical load on the tyre (F_z).

$$\begin{aligned} \lambda &= \frac{\mu F_z}{2C_\alpha \left|\tan(\alpha)\right|} \\ f(\lambda) &= \begin{cases} \lambda(2-\lambda) & \text{if } \lambda \le 1 \\ 1 & \text{if } \lambda > 1 \end{cases} \\ F_y &= -f(\lambda) C_\alpha \tan(\alpha). \end{aligned} \tag{5}$$

3 Experimental setup

The methods described in this paper are experimentally tested on the fully instrumented G35 sedan shown in Figure 2. The G35 is equipped with a dual antenna Novatel™ Beeline receiver that provides 5 Hz updates of vehicle heading, roll, speed, and course. It is also instrumented with a lateral accelerometer and yaw gyroscope recorded at 30 Hz. Additionally, wheel speed and steer angle are recorded from the onboard sensors through the CAN bus at 30 Hz. With the exception of the dual antenna GPS system, each of these sensors is available on any vehicle with ESC. The methods presented in this paper show the benefit of adding dual antenna GPS to ESC. The vehicle's mass (m) is 1528 kg; the yaw moment of inertia (I_z) is approximated as 2400 kg m^2 (Heydinger et al., 1999).

Figure 2 Instrumented infiniti G35 sedan

3.1 Test scenarios

Two experimental test scenarios are used to validate the methods presented in this paper: hard cornering on a low-μ gravel surface and limit driving on asphalt. The low-μ surface experiment steer angle and resulting yaw rate are shown in Figure 3. This experiment is run at an average speed of 6 m/s.

Figure 3 Low-μ experiment steer angle and yaw rate

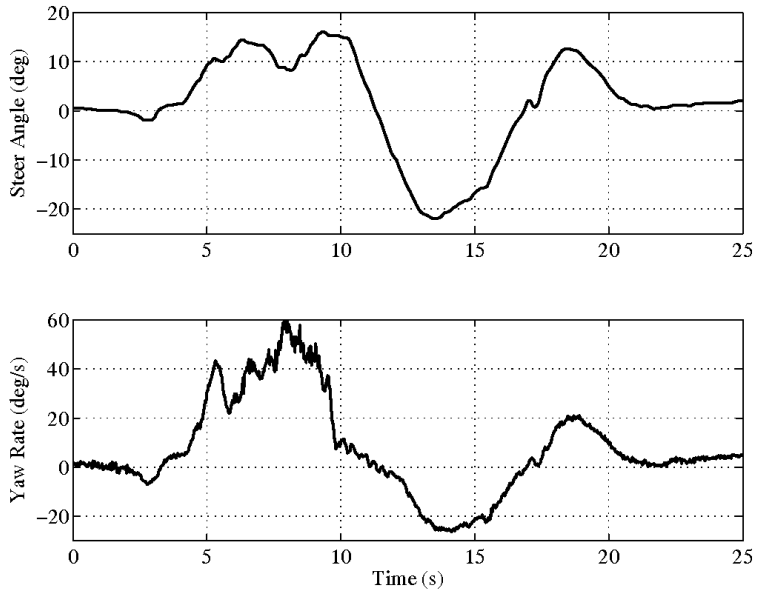

The asphalt scenario consists of three segments. The first is a high speed, steady state cornering experiment performed at 37 m/s around a 150 m radius turn banked at 8 deg. As in equation (2), the bank angle is typically neglected in vehicle models, but from equation (1), it does affect the sideslip. The second segment is a lane change performed at 20 m/s. The final segment is a slalom at 25 m/s. The steer angle and yaw rate for this experiment are shown in Figure 4.

Figure 4 Asphalt experiment steer angle and yaw rate

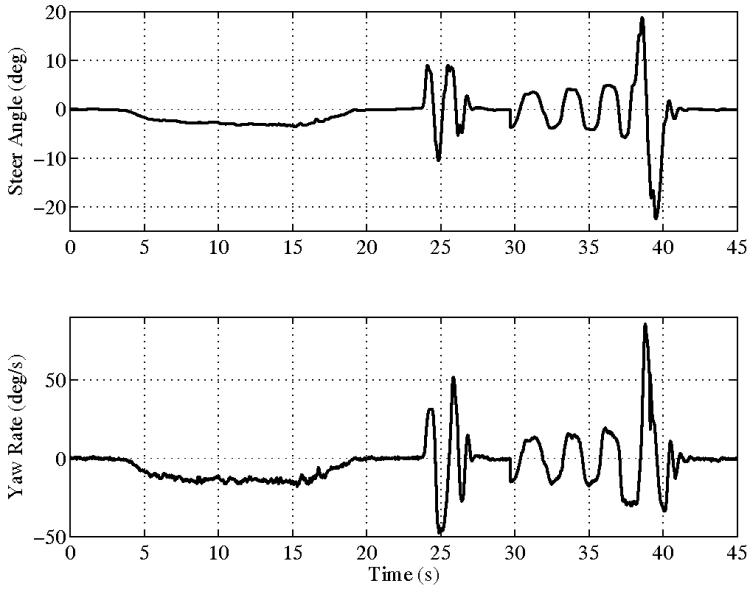

3.2 Sensor models

To utilise the various measurements properly, the models of the sensors must be understood. GPS provides noisy, but unbiased, measurements of vehicle course (with one antenna) and heading (with a two antenna system) as shown below.

$$\begin{aligned} \psi^{\langle \text{GPS} \rangle} &= \psi + \eta_\psi \\ v^{\langle \text{GPS} \rangle} &= v + \eta_v . \end{aligned} \tag{6}$$

The sampled noise on the GPS measurements is given in equation (7).

$$\begin{aligned} \sigma_\psi^2 &= \left(\frac{0.4\pi \text{ rad}}{180} \right)^2 \\ \sigma_v^2 &= \left(\frac{0.05 \text{ m/s}}{V} \right)^2 . \end{aligned} \tag{7}$$

Note that the accuracy of the course estimate will improve with speed (Daily and Bevly, 2004).

The gyroscope is modelled as having Gaussian noise and a moving bias that is modelled as a random walk.

$$\begin{aligned} r^{\langle \text{gyro} \rangle} &= r + b_{\text{gyro}} + \eta_r \\ \dot{b}_{\text{gyro}} &= w_{b_{\text{gyro}}} . \end{aligned} \tag{8}$$

This model, although quite simplistic, captures most of the error sources that affect vehicle state estimation. More complex inertial sensor models, which include scale factor errors as well as mis-alignment and cross-coupling errors, have been studied (Titterton and Weston, 1997), but are not the focus of this paper. The value of the gyroscope noise as well as the noise driving the bias are functions of the specific sensor used. Generally, as the sensor quality decreases these values increase (Gebre-Egziabher, 2004). The sampled noise values for the gyroscope used in this paper are

$$\begin{aligned} \sigma_r^2 &= \left(\frac{0.1\pi \text{ rad/s}}{180} \right)^2 \\ \sigma_{b_{gyro}}^2 &= (10^{-5} \text{ rad/s})^2 . \end{aligned} \tag{9}$$

Similarly, the accelerometer is modelled as having Gaussian noise and a random walk bias. Due to vehicle roll including bank angle (θ), the lateral accelerometer also contains the effect of the gravitational field in its measurements.

$$\begin{aligned} a_y^{\langle \text{accel} \rangle} &= a_y + g \sin(\theta) + b_{\text{accel}} + \eta_{a_y} \\ \dot{b}_{\text{accel}} &= w_{b_{\text{accel}}} . \end{aligned} \tag{10}$$

The sampled noise values for the accelerometer used in this paper are given below.

$$\begin{aligned} \sigma_{a_y}^2 &= (0.05 \text{ m/s}^2)^2 \\ \sigma_{b_{\text{accel}}}^2 &= (10^{-5} \text{ m/s}^2)^2 . \end{aligned} \tag{11}$$

4 Sideslip calculation

The body sideslip angle (β in Figure 1) is the angle between the longitudinal and lateral velocity components at the Centre of Gravity (CG).

$$\beta = \tan^{-1}\left(\frac{V_y}{V_x}\right). \tag{12}$$

A typical method to measure sideslip on test vehicles is using an optical sensor to measure the lateral and longitudinal velocity. However, these sensors are expensive and performance can be surface dependent. For these reasons, on production vehicles, this state is not measured.

A newer method to measure sideslip is using GPS. The sideslip angle can also be defined as the difference between the vehicle heading and direction of travel (course) measured at the CG.

$$\beta = \nu - \psi. \tag{13}$$

GPS provides a course measurement. However, the vehicle heading must still be determined. Heading can be estimated using a yaw gyro. The gyro is initialised and its bias estimated during periods of straight driving and then integrated during turning manoeuvres to provide the vehicle heading (Bevly et al., 2002). This technique has several drawbacks: Estimating an integrated signal is an unobservable process; mathematically the estimate error cannot be bound. Practically, this means errors such as incorrect biases or scale factors can cause large errors in the sideslip estimate. Another problem is aligning the time each measurement was taken. Inherent delay occurs between the time a GPS measurement is taken and the time the measurement is received by a computer. Depending on how the gyroscope measurement is taken, it may have a delay as well. Because vehicle sideslip is generally small (on the order of 1–2 deg), the two signals being subtracted in equation (13) must be aligned at precisely the same time to produce an accurate measurement (Bevly et al., 2001). Without an external signal (such as the GPS pulse per second), it is not easy to programmatically line up the two measurements.

Alternatively, the vehicle heading can be measured using two GPS antennas (Hong et al., 2001; Ryu et al., 2002). By utilising two antennas, heading estimate errors due to both gyro integration (arising from bias estimate errors, scale factor, integration routine, and integration of a noisy signal) and synchronisation of the GPS/INS measurements are eliminated. The GPS velocity measurements (including course) have a delay that is not present in the position measurements (including heading). The GPS velocity vector is calculated by comparing consecutive phase measurements of the carrier wave. When consecutive phase measurements are compared, the measurement has a half sample delay. This delay is similar to that introduced by a backward difference approximation. Unlike the GPS/IMU synchronisation, this delay is easy to account for programmatically.

The two methods (GPS and optical) are compared for the asphalt experiment in Figure 5 and match quite well; for the sake of scale, the slalom is not included. This validates the GPS method to compute sideslip presented above. Further validation using the optical sensor can be found in Rock et al. (2005) and Bevly et al. (2006). For the remainder of the paper, the GPS approach will be used for the sideslip measurement.

Figure 1 Asphalt experiment GPS slip angle validation with optical sensor

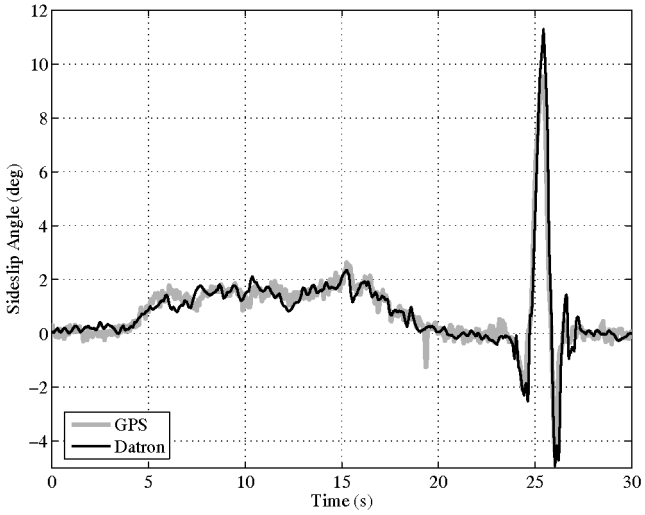

5 Kalman filter algorithm

This paper utilises a Kalman filter for the state estimation as opposed to other available observers (Brogan, 1991). The Kalman filter optimises the estimate by statistically weighting each measurement. An Extended Kalman Filter (EKF) is utilised for non-linear system models, and given a high sample rate is as accurate as some higher order filters and less computationally intensive (St. Pierre and Gingras, 2004). The cascaded estimation method presented in this paper utilises three Kalman filters: a kinematic state estimation, tyre parameter identification, and model-based state estimation. The algorithms for each of the estimators are the same, only the plant model changes. In particular, the algorithm used in this research is an extended Kalman-Bucy filter, outlined in detail by Stengal (1994). This algorithm handles the system non-linearities by continuously propagating the system model and discretely propagating the measurement update, as shown in the following equations.

State estimate continuous propagation

$$\hat{\mathbf{x}}(t_k^-) = \hat{\mathbf{x}}(t_{k-1}^+) + \int_{t_{k-1}}^{t_k} \mathbf{f}[\hat{\mathbf{x}}(\tau^-), \mathbf{u}(\tau), \tau]\, \mathrm{d}\tau. \tag{14}$$

Covariance estimate continuous propagation

$$\mathbf{P}(t_k^-) = \mathbf{P}(t_{k-1}^+) + \int_{t_{k-1}}^{t_k} [\mathbf{A}(\tau)\mathbf{P}(\tau) + \mathbf{P}(\tau)\mathbf{A}(\tau)^{\mathrm{T}}]\, \mathrm{d}\tau + \mathbf{Q}_d. \tag{15}$$

Kalman filter gain calculation

$$\mathbf{L}(t_k) = \mathbf{P}(t_k^-)\mathbf{C}(t_k)^{\mathrm{T}}[\mathbf{C}(t_k)\mathbf{P}(t_k^-)\mathbf{C}(t_k)^{\mathrm{T}} + \mathbf{R}_d(t_k)]^{-1}. \tag{16}$$

Residual calculation

$$\boldsymbol{\xi}(t_k^+) = \mathbf{y}(t_k) - \mathbf{C}(t_k)\hat{\mathbf{x}}(t_k^-). \tag{17}$$

State estimate discrete update

$$\hat{\mathbf{x}}(t_k^+) = \hat{\mathbf{x}}(t_k^-) + \mathbf{L}(t_k)\boldsymbol{\xi}(t_k^+). \tag{18}$$

Covariance estimate discrete update

$$\mathbf{P}(t_k^+) = [\mathbf{I} - \mathbf{L}(t_k)\mathbf{C}(t_k)]\mathbf{P}(t_k^-). \tag{19}$$

f is the system of differential equations defining the system. If the system is linear, **A** is simply the state transition matrix; if it is non-linear, **A** is given by the Jacobian of the system.

$$\mathbf{A}(t_k) = \nabla_{\mathbf{x}}\mathbf{f}\Big|_{\substack{\mathbf{x}(t_{k-1}) \\ \mathbf{u}(t_{k-1})}}. \tag{20}$$

$\mathbf{Q}_d$ and $\mathbf{R}_d$ are the discrete process and measurement noise covariances respectively. Expressions for each of these variables are given when the individual Kalman filter systems are defined.

6 Kinematic Kalman filter

The first step of the cascaded estimation approach utilises a kinematic Kalman filter to combine the GPS and inertial measurements to provide high-update rate, unbiased, accurate estimates of the lateral vehicle dynamics (Bevly et al., 2001). The term *kinematic* comes from the fact that the model used by the estimator is based solely on the kinematic relationship between the sensors and not a dynamic model of the vehicle. For this filter, the linearised form of the Kalman filter described in equations (14)–(19) is used to estimate the states. The models for the gyroscope in equation (8) and lateral accelerometer in equation (10) can be combined with the measurements from a two-antenna GPS system to form the kinematic state space relationships given below.

$$\begin{aligned}
\mathbf{f} &= \begin{bmatrix} \dot{\psi} \\ \dot{\beta} \\ \dot{b}_{\text{gyro}} \\ \dot{b}_{\text{accel}} \end{bmatrix} = \begin{bmatrix} 0 & 0 & -1 & 0 \\ 0 & 0 & 1 & -1/V_x \\ 0 & 0 & 0 & 0 \\ 0 & 0 & 0 & 0 \end{bmatrix} \begin{bmatrix} \psi \\ \beta \\ b_{\text{gyro}} \\ b_{\text{accel}} \end{bmatrix} + \begin{bmatrix} 1 & 0 \\ -1 & 1/V_x \\ 0 & 0 \\ 0 & 0 \end{bmatrix} \begin{bmatrix} r^{\langle \text{gyro} \rangle} & a_y^{\langle \text{corrected} \rangle} \end{bmatrix} + \mathbf{w} \\
\mathbf{y} &= \begin{bmatrix} \psi^{\langle \text{GPS} \rangle} \\ v^{\langle \text{GPS} \rangle} \end{bmatrix} = \begin{bmatrix} 1 & 0 & 0 & 0 \\ 1 & 1 & 0 & 0 \end{bmatrix} \begin{bmatrix} \psi \\ \beta \\ b_{\text{gyro}} \\ b_{\text{accel}} \end{bmatrix} + \boldsymbol{\eta}.
\end{aligned} \tag{21}$$

The estimator adjusts the accelerometer bias estimate to compensate for any roll measured by the lateral accelerometer. However, the two-antenna GPS system provides a roll measurement that can be used to correct the lateral acceleration.

$$a_y^{\langle \text{corrected} \rangle} = a_y^{\langle \text{accel} \rangle} - g\sin(\theta). \tag{22}$$

The sensor noise and process noise covariance matrices for the above system are given below.

$$\mathbf{R_d} = \begin{bmatrix} \sigma_\psi^2 & 0 \\ 0 & \sigma_v^2 \end{bmatrix}$$

$$\mathbf{Q_d} = \begin{bmatrix} T_s^2\sigma_r^2 & -T_s^2\sigma_r^2 & 0 & 0 \\ -T_s^2\sigma_r^2 & T_s^2(\sigma_r^2 + (\sigma_{a_y}^2 / V_x^2)) & 0 & 0 \\ 0 & 0 & \sigma_{b_{\text{gyro}}}^2 & 0 \\ 0 & 0 & 0 & \sigma_{b_{\text{accel}}}^2 \end{bmatrix} \tag{23}$$

T_s is the sample rate of the Kalman filter inputs. Figure 6 shows the estimates of sideslip and heading, for the low-μ and asphalt tests described previously.

Figure 6 Estimates using the kinematic Kalman filter

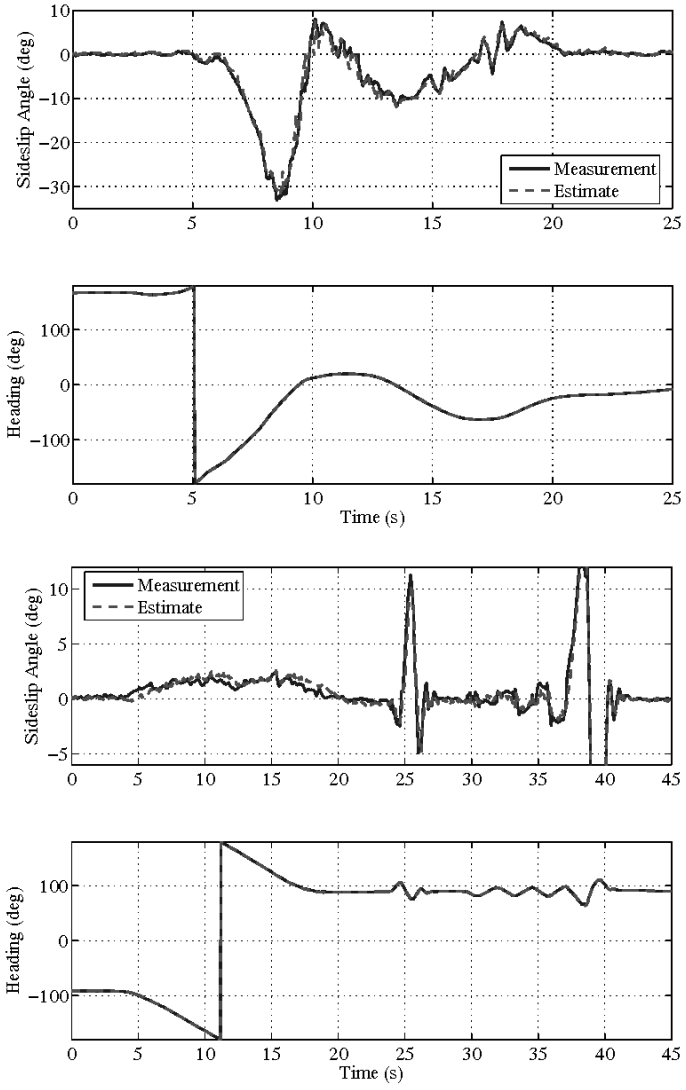

7 Tyre parameter identification

Using the state estimates from the kinematic Kalman filter, the tyre curve for each axle can be generated and tyre parameters estimated. Because no small angle approximations are used in the kinematic Kalman filter plant model, the estimates are valid beyond the linear region of the tyre. Several researchers have produced experimental tyre curves using various methods (such as steering wheel torque) to estimate the lateral force at the tyre (Koo et al., 2004; Switkes and Gerdes, 2005; Hsu and Gerdes, 2005; M'Sirdi et al., 2005). Other researchers have developed methods to estimate peak coefficient of friction (Ray, 1995; Müller et al., 2003), including methods which utilise GPS (Hahn and Rajamani, 2002). In this paper, simple Newtonian dynamics are used to accomplish the force estimation. The lateral acceleration and yaw rate estimates can be used to determine the front and rear axle lateral forces.

$$\begin{aligned} \sum F_y &= ma_y = F_{yr} + F_{yf}\cos(\delta) \\ \sum M_z &= I_z\ddot{\psi} = -bF_{yr} + aF_{yf}\cos(\delta). \end{aligned} \tag{24}$$

Several assumptions are made in these equations. First, longitudinal forces are ignored. The only longitudinal force that might appear is from the front tyre due to the steer angle. Unless the vehicle is braking, this force will be negligible for rear wheel drive vehicles (such as the G35). It is possible to add a longitudinal acceleration/force equation and make an assumption about the brake bias to include braking and driving forces. If the vehicle is undergoing significant acceleration or braking, the additional forces should be included so the lateral estimation does not become corrupted by the neglected longitudinal terms. Including longitudinal forces also allows the longitudinal tyre curve to be predicted; however, it is beyond the scope of this paper.

The lateral forces in the equations are per axle, not per tyre; the lateral force on an axle is simply the sum of the lateral forces from each of the tyres on that axle. The equations include the second derivative of heading. To determine this measurement, the yaw rate gyroscope must be numerically differentiated; the differentiation may add lag and noise that can corrupt the estimation. Using the tyre sideslip measurements presented above and these lateral forces, it is possible to predict the lateral tyre curves for the vehicle. The tyre curves can then be used to estimate parameters for the various tyre models available.

Although many researchers have estimated tyre cornering stiffness online using linear tyre models, to predict the tyre behaviour outside the linear region, a more complicated model such as the Dugoff model, equation (5), must be used. The Dugoff model has two parameters to identify for each tyre: cornering stiffness and peak lateral force (peak coefficient of friction multiplied by vertical load). As with the linear model, it is safe to assume the inner and outer cornering stiffnesses are equal; the inner and outer coefficients of friction are also equal. However, this model includes (and is not linear in) vertical force; assuming no weight transfer is not always practical.

Because the Dugoff model is not linear in vertical force, it is not immediately apparent mathematically that it is possible to identify a 'lumped' peak force for the axle. This problem can be visualised in the transition region of the model. With this model it is possible to have the outer tyre in the linear region ($\lambda > 1$) and the inner tyre beginning to saturate ($\lambda < 1$) due to more vertical load on the outer tyre. However, it is normally safe to assume that the concept of the Dugoff model works for an axle as well as for a tyre;

the axle will have a cornering stiffness and a peak lateral force. The Dugoff model of the axle captures these two characteristics. This assumption may break down in vehicles with large roll angles however, particularly if the roll dynamics are not significantly faster than the yaw dynamics, i.e., weight transfer for a given slip angle cannot be considered constant. In this case, the peak lateral force for the axle would not be constant.

For vehicles with large amounts of roll, this presents opportunities as well as difficulties. If cornering stiffness and coefficient of friction are assumed equal for the inner and outer tyres and the total vertical load on all the tyres is constant (vehicle weight), it should be possible to identify the vertical load on each tyre as well as the tyre parameters by summing the lateral forces for each axle. However, the vehicle used in this paper does not exhibit significant weight transfer; thus, there is not enough excitation to identify the tyre loads separately.

Because the Dugoff model is non-linear, simple techniques such as Recursive Least Squares (RLS) do not work to identify the parameters. However, researchers have used a modified Dugoff model to incorporate RLS (Kwak et al., 2000). A more complicated non-linear technique, such as an extended Kalman filter, must be used for the non-linear Dugoff model. The Kalman filter is presented in equations (14)–(19); the only difference is the state (parameter estimates) does not vary with time.

$$\begin{aligned} \mathbf{f} &= \begin{bmatrix} \dot{C}_\alpha \\ (\mu^{-} F_z) \end{bmatrix} = \mathbf{w} \\ \mathbf{y} &= [F_y] = \mathbf{C} \begin{bmatrix} C_\alpha \\ (\mu F_z) \end{bmatrix} + \boldsymbol{\eta}. \end{aligned} \tag{25}$$

The measurement is lateral force, so the output matrix (**C**) is the gradient of the Dugoff model with respect to the parameters.

$$\begin{aligned} \lambda(t_k) &= \frac{(\mu F_z)_{k-1}}{2C_{\alpha k-1} \left|\tan(\alpha_k)\right|} \\ \mathbf{C}(t_k) &= \begin{cases} \begin{bmatrix} \dfrac{-(\mu F_z)_{k-1}^2}{4C_{\alpha k-1}^2 \tan(\alpha_k)} & \dfrac{(\mu F_z)_{k-1}}{2C_{\alpha k-1} \tan(\alpha_k)} - \operatorname{sign}(\tan(\alpha_k)) \end{bmatrix} & \text{if } \lambda(t_k) \le 1 \\ \begin{bmatrix} -\tan(\alpha_k) & 0 \end{bmatrix} & \text{if } \lambda(t_k) > 1 \end{cases}. \end{aligned} \tag{26}$$

The process noise covariance ($\mathbf{Q}_d$) acts like a forgetting factor, allowing the estimated parameters to change over time. For this work, the process and measurement noise covariances are chosen to be

$$\begin{aligned} \mathbf{R}_d &= (1000 \text{ N})^2 \\ \mathbf{Q}_d &= 10^{-8} \begin{bmatrix} (80000 \text{ N/rad})^2 & 0 \\ 0 & (15000 \text{ N})^2 \end{bmatrix}. \end{aligned} \tag{27}$$

Another way to think of the recursion algorithm is as recursive least squares where the regression matrix is defined like the output matrix in the Kalman filter.

The parameter identification algorithm is validated on the two experimental runs described above. Figure 7 shows the asphalt experiment. There appears to be multiple fits due to the estimation algorithm adapting over time. The raw data also seem to have this behaviour implying the parameters are varying with time. In particular, the rear tyre

saturates at approximately 7 kN but distinctly goes above this lateral force at –5 deg of slip. This discrepancy could be due to weight transfer. Slip angles beyond –7 deg are only seen near the end of the slalom portion. This manoeuvre is violent enough that weight transfer was significant. The other two portions of the experiment (steady state cornering and lane changes) are not that violent and thus do not have the weight transfer. The estimation algorithm is adaptive enough to capture the different behaviours at different times during the experiment.

Figure 7 Estimated tyre curves from the asphalt experiment

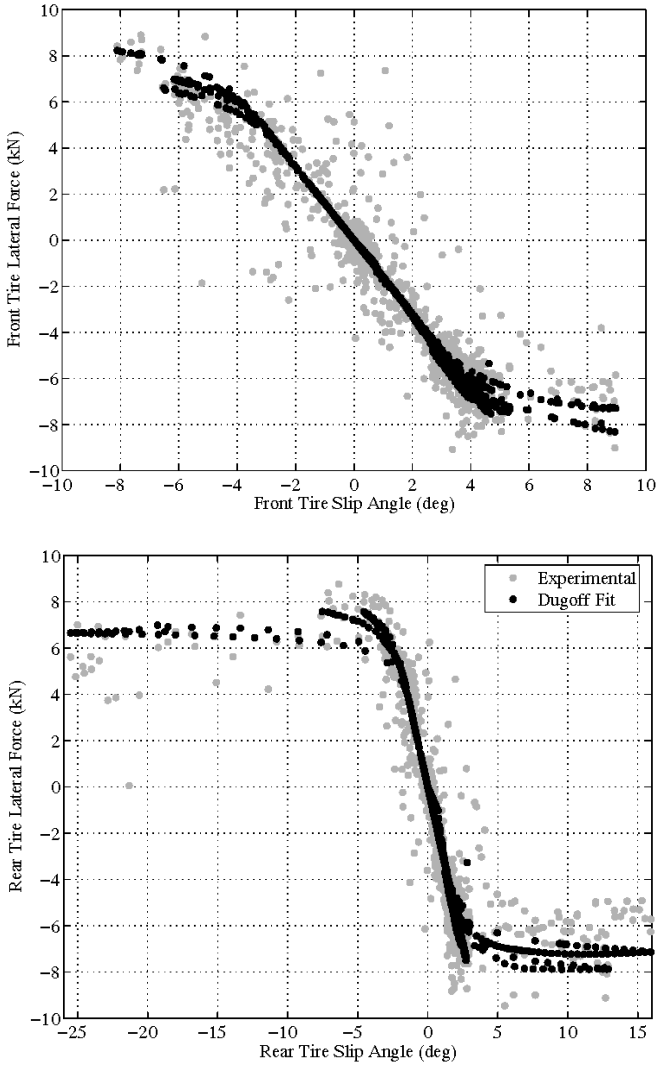

Figure 8 shows the parameter estimation throughout the asphalt experiment. The Kalman filter (recursive) is compared to a non-linear batch least squares performed over the entire experiment. For the most part, the recursion converges near the batch estimation. The notable exception to this is the front cornering stiffness; the recursion

remains lower than the batch estimation. Although this difference looks significant as plotted, the difference in slope represented on the tyre curve is not very noticeable. Either could be judged as a valid fit.

Figure 8 Estimated tyre parameters from the asphalt experiment

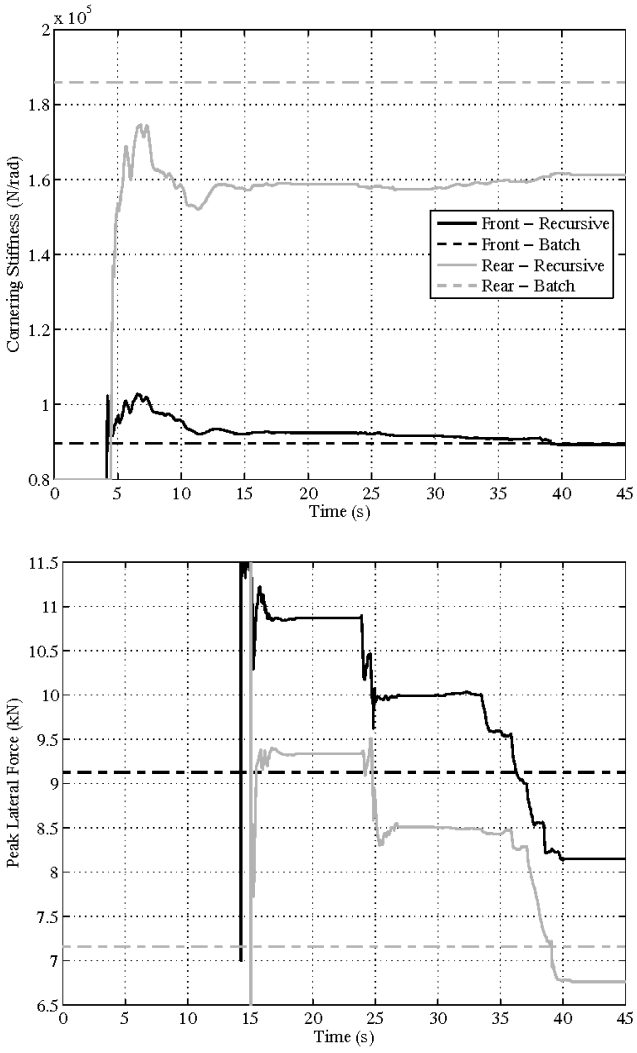

The peak lateral force estimate portrays an aspect of the Kalman filter that is quite useful in this application. Most parameter identification schemes require a switch to determine when to estimate solely the cornering stiffness vs. estimating both parameters, i.e., when the tyre is beginning to saturate. When the tyre is in the linear region ($\lambda > 1$), the Dugoff model (and thus the Kalman filter output matrix) does not contain the peak force; this parameter is unobservable. When the Kalman filter encounters an unobservable state, it sets the gain on that state to zero in this case meaning hold the parameter constant. Therefore, when the tyre is operating in the linear region, the Kalman filter automatically holds the peak force at the last estimated value. This is the reason for the

many plateaus in the peak force estimate. The tyre only enters the non-linear region for short periods at a time; the first of these is exiting the corner. During these short intervals, the peak force estimate is updated; otherwise, it is simply held constant.

Figure 9 shows the measured tyre curve along with the estimated Dugoff fit for the low-μ experiment. Filtered measurements are shown along with the unfiltered measurements and curve fit; the curve fit utilises the unfiltered measurements. The reason for the filtered measurements is to show graphically that the curve fit appears to identify the most reasonable parameters for the tyre. As with the asphalt experiment, the parameters appear to vary with time (there appear to be multiple curve fits); this is due in part to weight transfer as it was in the asphalt experiment. The changing parameters are also due in part to the irregularity in the gravel surface itself. In addition, the measured force (even after filtering) is very noisy due to the rough gravel surface, but the estimation scheme effectively averages the noise out. The parameters identified in this experiment are successfully used in the model-based filter below, showing that even in the presence of a large signal to noise ratio the identification and estimation schemes perform well together. The estimated parameters exhibit similar behaviour to the asphalt experiment and so are not shown.

Figure 9 Estimated tyre curves from the low-μ test

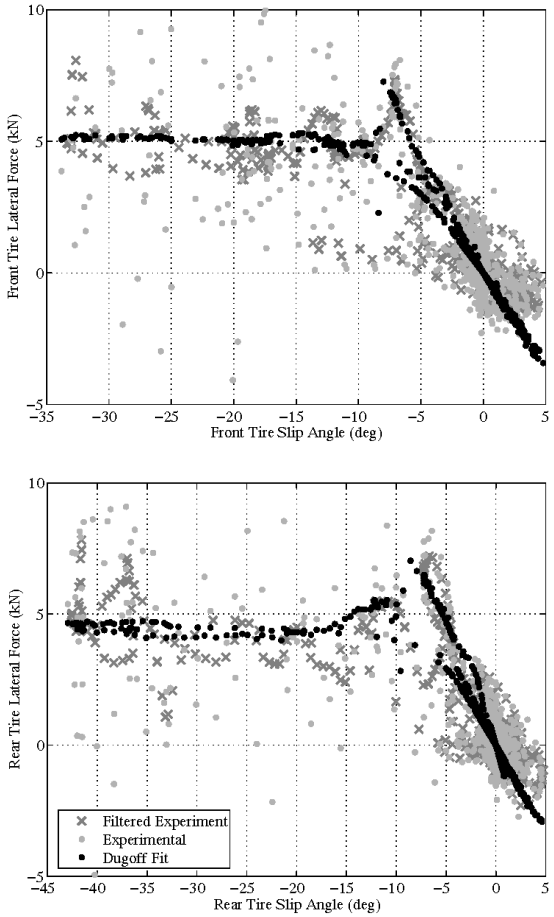

Another important consideration when estimating the tyre parameters is the initial guess of peak force. To obtain an accurate estimate, the initial peak force guess must be higher than the actual value. In an extreme sense, if the peak force estimate is too low, the estimator is constantly receiving measurements of lateral force above the peak and so continually moves the estimate of peak force up to the measured value. However, the Kalman filter also believes the estimate cannot change quickly (based on $\mathbf{Q}_d$), and so it becomes 'harder' to move the estimate. Ultimately, the estimate of peak force will always be lower than the truth and even the highest measured forces.

This problem is easy to circumvent by initially guessing the peak force unreasonably high. This does not cause any problems in the estimator because while the tyre is in the linear region, the peak force does not come into play. As soon as the tyre begins to saturate for the first time (t = 15 s in Figure 8), the peak force estimate drops immediately to a reasonable value.

8 Model-based Kalman filter

8.1 Linear tyre model

Once the tyre parameters have been identified, the GPS measurements can be combined with the inertial sensors using a model-based estimator. The estimator's state space model is derived from the linearised bicycle model given in equation (2). This Kalman filter form is called a model-based estimator because the vehicle model is used in the state matrices for the estimator. The state space equations for the model-based estimator, including the heading and gyro bias, are shown in equation (28).

$$\begin{aligned}\mathbf{f} &= \begin{bmatrix} \dot{\beta} \\ \dot{r} \\ \dot{\psi} \\ \dot{b}_{\text{gyro}} \\ \dot{b}_{\text{accel}} \end{bmatrix} = \begin{bmatrix} (-C_{\alpha f} - C_{\alpha r})/mV & (-aC_{\alpha \text{f}} + bC_{ar})/mV^2 - 1 & 0 & 0 & 0 \\ (-aC_{\alpha f} + bC_{\alpha r})/I_z & (-a^2C_{\alpha f} - b^2C_{\alpha r})/I_z V & 0 & 0 & 0 \\ 0 & 1 & 0 & 0 & 0 \\ 0 & 0 & 0 & 0 & 0 \\ 0 & 0 & 0 & 0 & 0 \end{bmatrix} \begin{bmatrix} \beta \\ r \\ \psi \\ b_{\text{gyro}} \\ b_{\text{accel}} \end{bmatrix} \\ &+ \begin{bmatrix} C_{af}/mV \\ aC_{\alpha f}/I_z \\ 0 \\ 0 \\ 0 \end{bmatrix} \delta + \mathbf{w} \end{aligned} \tag{28}$$

$$\mathbf{y} = \mathbf{C} \begin{bmatrix} \beta \\ r \\ \psi \\ b_{\text{gyro}} \\ b_{\text{accel}} \end{bmatrix} + \mathbf{D}\delta + \boldsymbol{\eta}$$

The output equations for this model (as well as which states are observable) depend on the sensors used. Table 1 provides the various states (and the associated C and D matrices) that are observable given the measurements available to the model-based

estimator. Farrelly and Wellstead (1996) has shown how to incorporate a lateral accelerometer measurement into the model-based estimator that results in the following state space description of the system. If used, the lateral accelerometer measurement must be compensated for roll as shown in equation (22).

These estimators provide a direct estimate of the sideslip (β), yaw rate (r), and vehicle heading (ψ). Some configurations estimate the gyroscope and/or accelerometer biases (b_{gyro} and b_{accel}). The input into the estimators is the steer angle at the wheel (δ). Measurements include yaw rate plus bias (from a gyroscope), the course angle (from GPS), vehicle heading (from two antenna GPS), and lateral acceleration plus bias (from a lateral accelerometer). Note, as shown in equation (4), vehicle sideslip is not observable using only a yaw rate measurement if the vehicle model is neutral steer. However, sideslip remains observable with GPS measurements for a neutral steer vehicle.

Table 1 Kalman filter sensor options

Case	*Sensors*	*C matrix*	*D matrix*	*Observable*
1	1 ant GPS	$\begin{bmatrix}1 & 0 & 1 & 0 & 0\end{bmatrix}$	$\begin{bmatrix}0\end{bmatrix}$	β, r, ψ
2	1 ant GPS, yaw gyro	$\begin{bmatrix}1 & 0 & 1 & 0 & 0\\ 0 & 1 & 0 & 1 & 0\end{bmatrix}$	$\begin{bmatrix}0\\0\end{bmatrix}$	$\beta, r, \psi, b_{\text{gyro}}$
3	2 ant GPS	$\begin{bmatrix}1 & 0 & 1 & 0 & 0\\ 0 & 0 & 1 & 0 & 0\end{bmatrix}$	$\begin{bmatrix}0\\0\end{bmatrix}$	β, r, ψ
4	2 ant GPS, yaw gyro	$\begin{bmatrix}1 & 0 & 1 & 0 & 0\\ 0 & 1 & 0 & 1 & 0\\ 0 & 0 & 1 & 0 & 0\end{bmatrix}$	$\begin{bmatrix}0\\0\\0\end{bmatrix}$	$\beta, r, \psi, b_{\text{gyro}}$
5	yaw gyro	$\begin{bmatrix}0 & 1 & 0 & 1 & 0\end{bmatrix}$	$\begin{bmatrix}0\end{bmatrix}$	$\beta, r, b_{\text{gyro}}$*
6	yaw gyro, lat accel	$\begin{bmatrix}0 & 1 & 0 & 1 & 0\\ (-C_{\alpha f}-C_{\alpha r})m & (-aC_{\alpha f}+bC_{ar})/mV & 0 & 0 & 1\end{bmatrix}$	$\begin{bmatrix}0\\C_{af}/m\end{bmatrix}$	$\beta, r, b_{\text{gyro}}, b_{\text{accel}}$
7	1 ant GPS, lat accel	$\begin{bmatrix}1 & 0 & 1 & 0 & 0\\ (-C_{\alpha f}-C_{\alpha r})/m & (-aC_{\alpha f}+bC_{ar})/mV & 0 & 0 & 1\end{bmatrix}$	$\begin{bmatrix}0\\C_{af}/m\end{bmatrix}$	$\beta, r, \psi, b_{\text{accel}}$
8	1 ant GPS, yaw gyro, lat accel	$\begin{bmatrix}1 & 0 & 1 & 0 & 0\\ 0 & 1 & 0 & 1 & 0\\ (-C_{\alpha f}-C_{ar})/m & (-aC_{\alpha f}+bC_{ar})/mV & 0 & 0 & 1\end{bmatrix}$	$\begin{bmatrix}0\\0\\C_{af}/m\end{bmatrix}$	$\beta, r, \psi, b_{\text{gyro}}, b_{\text{accel}}$
9	2 ant GPS, lat accel	$\begin{bmatrix}1 & 0 & 1 & 0 & 0\\ 0 & 0 & 1 & 0 & 0\\ (-C_{\alpha f}-C_{ar})/m & (-aC_{\alpha f}+bC_{ar})/mV & 0 & 0 & 1\end{bmatrix}$	$\begin{bmatrix}0\\0\\C_{af}/m\end{bmatrix}$	$\beta, r, \psi, b_{\text{accel}}$
10	2 ant GPS, yaw gyro, lat accel	$\begin{bmatrix}1 & 0 & 1 & 0 & 0\\ 0 & 1 & 0 & 1 & 0\\ 0 & 0 & 1 & 0 & 0\\ (-C_{\alpha f}-C_{\alpha r})/m & (-aC_{\alpha f}+bC_{ar})/mV & 0 & 0 & 1\end{bmatrix}$	$\begin{bmatrix}0\\0\\0\\C_{af}/m\end{bmatrix}$	$\beta, r, \psi, b_{\text{gyro}}, b_{\text{accel}}$

*If the vehicle is not neutral steer.

The discrete processes noise covariance is shown in equation (29).

$$\mathbf{Q}_d = \begin{bmatrix} (0.1\pi \text{ rad}/180)^2 & 0 & 0 & 0 & 0 \\ 0 & (0.1\pi \text{ rad/s})^2 & 0 & 0 & 0 \\ 0 & 0 & (0.1\pi \text{ rad}/180)^2 & 0 & 0 \\ 0 & 0 & 0 & (10^{-5} \text{ rad/s})^2 & 0 \\ 0 & 0 & 0 & 0 & (10^{-5} \text{ m/s}^2)^2 \end{bmatrix} \tag{29}$$

Note that the actual transformation from process noise on the steer angle to state process noise must propagate through the input matrix. However, it may be better to 'hand-tune' the process noise covariance matrix to account for model parameter errors in the estimator model, resulting in the covariance above. Also, note that the estimator dynamics will change with the magnitude of the noise on the bias states, but that change is not a focus of this paper. The measurement noise covariance depends on the sensors used; like the other measurement noise covariance shown in the paper, it is diagonal and made up of the individual sensor noise variances.

Figure 10 shows the results of the sideslip estimation using the linear model-based estimator with the two antenna GPS measurements and a yaw rate gyro (Case 4). As seen in the figure, the linear estimator does a good job of estimating the sideslip around the turn of the track, even in the presence of the 8 deg road bank, and during the first part of the lane change and slalom manoeuvres. However, as would be expected with a linear estimator, it does not perform adequately during the more extreme manoeuvres when the vehicle begins to operate in the non-linear region of the tyre.

Figure 10 Sideslip estimate during the asphalt experiment using the linear model-based estimator (Case 4)

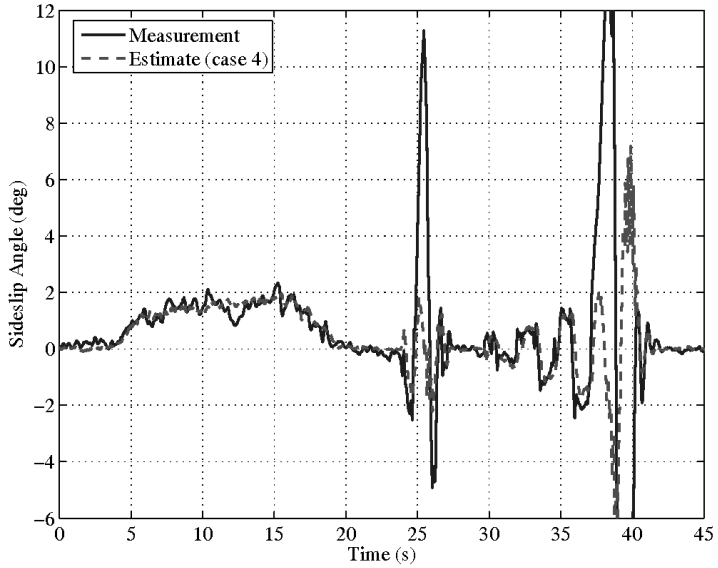

8.2 Non-linear tyre model

The model-based estimator can be improved by using the Dugoff (or other non-linear) tyre model to more accurately capture the non-linear effects of the tyre. The full non-linear dynamic model given in equation (1), in conjunction with the Dugoff tyre model given in equation (5), are used in the state estimation continuous propagation step of the estimator, equation (14), (i.e., to calculate **f**). For the remainder of the estimator steps, instead of computing the Jacobian of the full non-linear model, equation (20), the state transition matrix is approximated. For each tyre, the slope of the Dugoff model is computed at the current slip angle (α_o). These slopes become the cornering stiffnesses in the state transition matrix, equation (2). The slope of the Dugoff tyre model is

$$C'_\alpha(\alpha) = \left.\frac{dF_y}{d\alpha}\right|_{\alpha_o} = \begin{cases} -\dfrac{\mu^2 F_z^2}{4C_\alpha}\csc^2(\alpha) & \text{if } \lambda \le 1 \\ -C_\alpha \sec^2(\alpha) & \text{if } \lambda > 1 \end{cases}. \tag{30}$$

Figure 11 shows the slalom portion of the asphalt run compared to the simulated vehicle model using the Dugoff tyre model. The peak force and tyre cornering stiffness are taken from the non-linear tyre curve estimation shown in Figure 7. In simulation, the vehicle model with the Dugoff tyre parameters is able to capture the initial slide of the vehicle (as seen in the sideslip and yaw rate plots) but becomes unstable at the end of the run. However, as seen in Figures 12 and 13, the non-linear model-based estimator is still able to accurately estimate the states through the entire manoeuvre. Figure 12 shows the estimation results using only the yaw rate and lateral acceleration measurements (Case 6), while Figure 13 shows the estimation results with the addition of the two antenna GPS measurements (Case 4). Note the improvement of the sideslip estimates with the addition of the GPS measurements.

Figure 11 Sideslip and yaw rate during slalom section of the asphalt experiment

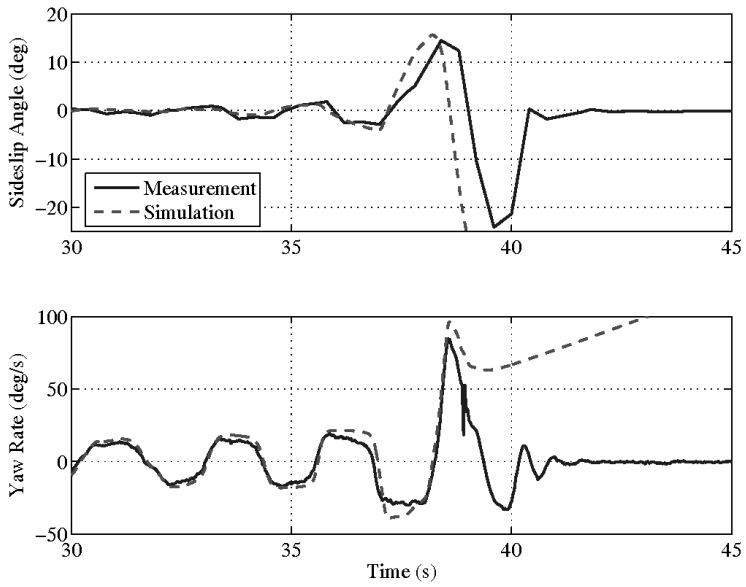

Figure 12 Sideslip estimate (Case 6) during asphalt experiment using model estimation with only yaw rate and lateral acceleration measurements

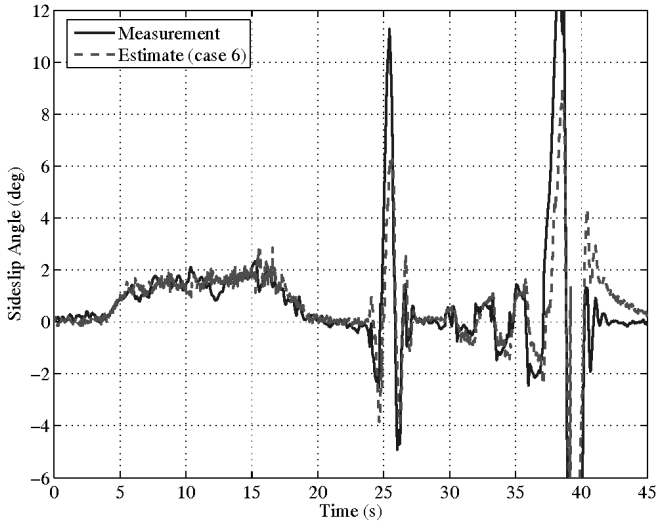

Figure 13 Sideslip estimate (Case 4) during asphalt experiment using two antenna GPS system

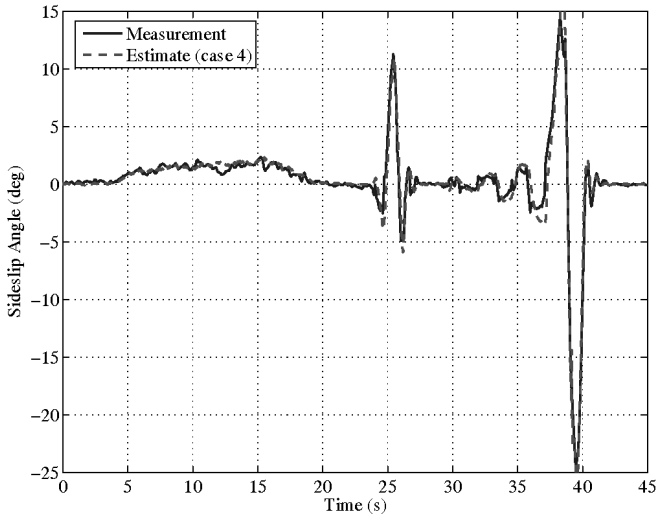

To test the robustness of the model-based estimator, it is run with incorrect vehicle parameters. The vehicle parameters are chosen such that the incorrect vehicle model has the same understeer gradient, equation (3), as the G35 (since vehicle understeer is fairly easy to estimate online. As seen in Figure 14, the model estimator (Case 4) with the incorrect model is able to accurately estimate the yaw rate through the turn, lane change, and part of the slalom. However, as seen in the figure, the sideslip estimation error is quite significant. Figure 15 shows the measurement residuals (ξ) from the Kalman filter estimator as described in equation (17). Note that the yaw rate measurement residual appears to be fairly random and centred about zero. However, inspection of the GPS measurement residuals provides a clear indication that there are errors in the

Kalman filter model. This shows the benefit of the GPS measurements (from one or two antenna systems) to provide a level of confidence in the estimated states and the model associated with the estimator. Additionally, these figures demonstrate the importance of accurate knowledge of the front and rear tyre parameters and not simply the understeer gradient of the vehicle.

Figure 14 Sideslip estimate during a series of manoeuvres using an incorrect model (Case 4)

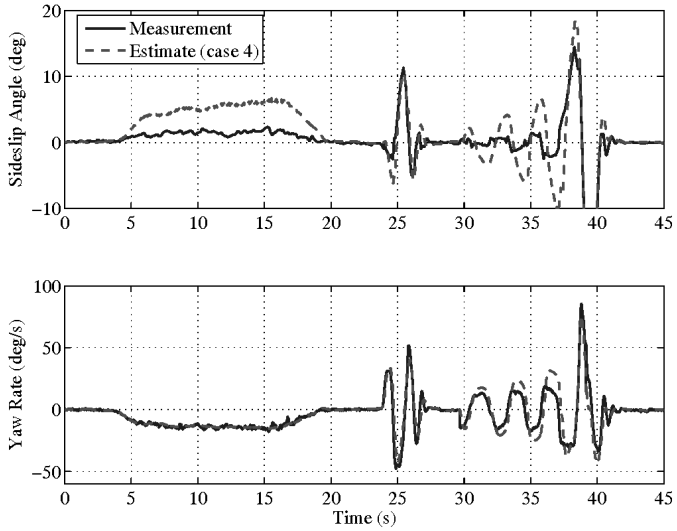

Figure 15 Measurement residuals during a series of manoeuvres using an incorrect model (Case 4)

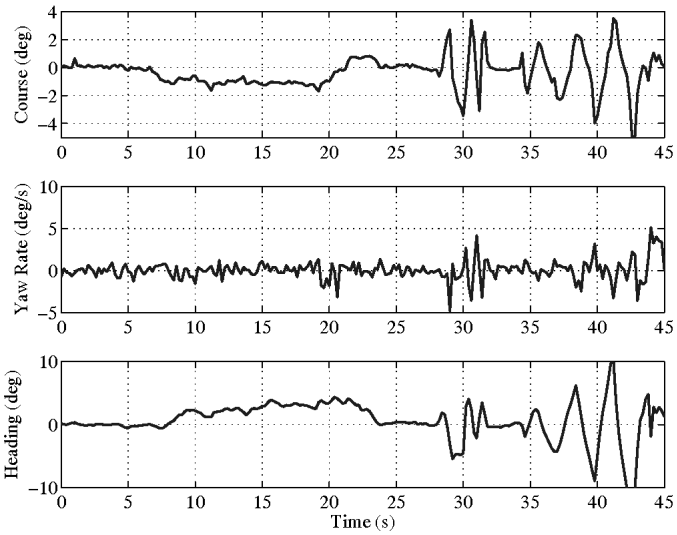

Finally, the non-linear model-based estimator is tested on the low-μ gravel surface described previously. Figure 16 shows the results of the non-linear model-based estimator (Case 4) using the Dugoff tyre parameters from the asphalt experiment. Notice that although the estimator provides a fairly good estimate of yaw rate during this experiment,

it does not capture the large sideslip from the vehicle slide on the low-μ surface. This demonstrates the importance of accurate peak tyre force in the model-based estimators. Figure 17 shows the sideslip estimation (Cases 4 and 6) results using the correct Dugoff low-μ tyre parameters, represented by Figure 9. The estimation results with only inertial sensor measurements (yaw rate and lateral accelerometer) compared to the results with the two antenna GPS measurements are shown. Note that even with the correct model parameters, the yaw rate gyroscope and lateral accelerometer are unable to estimate the large slip angle produced in this manoeuvre. However, the addition of the GPS measurements allows the model-based estimator to accurately capture the sideslip angle.

Figure 16 Sideslip estimate (Case 4) during a hard right turn on a low-μ surface using incorrect Dugoff tyre parameters

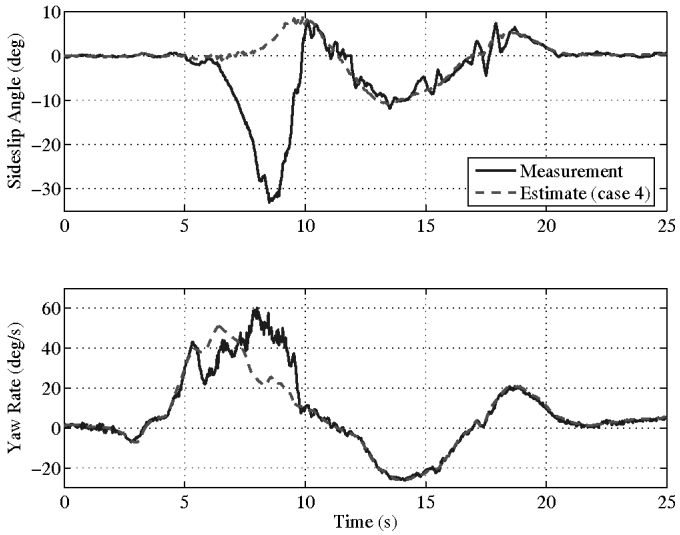

Figure 17 Sideslip estimate (Cases 4 and 6) during a hard right turn on a low-μ surface using the correct Dugoff tyre parameters

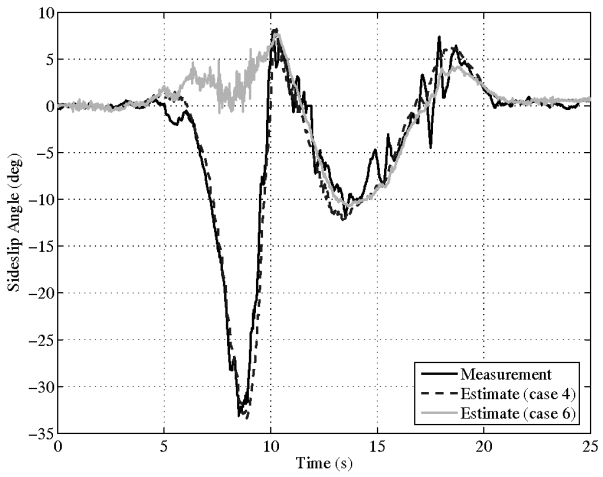

8.3 Estimator accuracies

To show the benefit of identifying the tyre parameters and re-estimating the vehicle states with a model-based estimator, a simple covariance analysis can be performed to determine the accuracy of the various estimation algorithms (Bevly et al., 2006). A summary of the covariance analysis (given in terms of the $1-\sigma$ values) is shown in Table 2. It is important to note that the covariance values for the kinematic Kalman filter assume there are no unmodelled sensor dynamics in the system (since the kinematic Kalman filter only depends on integration of sensor measurements). Also, note that the accuracy of these estimates will improve with speed as seen in equation (7). To improve the overall accuracy of the estimates, more comprehensive kinematic relationships could be added to reduce errors induced by roll and pitch.

The covariance values given for the model-based Kalman filter assume there are no unmodelled vehicle or sensor dynamics in the system (since the model-based Kalman filter depends on the integration of sensor measurements with the vehicle model). The analysis given in Table 2 is dependent primarily on the INS sensors, such as sensor noise and bias stability, and not the vehicle model. Also note that while it is not discussed in this paper, the model-based estimator provides better estimates in the presence of gyroscopic scale factor errors (if the correct vehicle parameters are used) or in the presence of banked roads (Anderson and Bevly, 2004).

Table 2 Covariance analysis summary (Max $1-\sigma$ values) at 8 m/s

Estimated state (*sensors used*)	*2-antenna* (KKF) (deg)	*Model-based Kalman filter* (deg)
Vehicle heading (GPS only)	0.4	0.03
Vehicle heading (GPS and yaw gyro)	0.1	0.01
Vehicle course (GPS only)	0.36	0.36
Vehicle slip angle (GPS only)	0.54	0.25
Vehicle slip angle (GPS and yaw gyro)	0.37	0.2
Vehicle slip angle (GPS, yaw gyro, and lat accel)	0.28	0.05

9 Conclusions

This paper has shown the ability of cascaded estimators (utilising GPS and inertial measurements) to provide accurate estimates of vehicle states for use in ESC Systems. A method for using these measurements to obtain Dugoff tyre parameters was provided. The method was tested using experimental data on high and low friction surfaces to verify the algorithms were robust to parameters changing with ground conditions. A covariance analysis provided the theoretically achievable accuracy, and results showed an improvement when using the estimates from the model-based estimator over a kinematic Kalman filter. These improved state estimates can be used to develop a more reliable and robust ESC system. Although the model-based estimator can provide vehicle information during a GPS outage, the kinematic Kalman filter can only provide reliable sideslip information for short periods without GPS measurements. Future work will investigate how this impacts the model-based Kalman filter as well as other methods to improve sideslip estimation.

Acknowledgements

The authors would like to thank Nissan Technical Center, North America for the loan of the Infiniti G35 sedan for the vehicle tests. Additionally, the authors would like to thank Delphi for the loan of the Datron™ velocity sensor used for validating some of the GPS/INS sideslip measurements. Any opinions, findings, conclusions, or recommendations expressed in this publication are those of the authors and do not necessarily reflect the views of Nissan or Delphi.

References

Anderson, R. and Bevly, D.M. (2004) 'Estimation of slip angles using a model based estimator and GPS', *Proceedings of the American Control Conference 2004*, pp.2122–2127.

Bevly, D.M., Sheridan, R. and Gerdes, J.C. (2001) 'Integrating INS sensors with GPS velocity measurements for continuous estimation of vehicle sideslip and tire cornering stiffness', *Proceedings of the American Control Conference 2001*, Vol. 1, pp.25–30.

Bevly, D.M., Gerdes, J.C. and Wilson, C. (2002) 'The use of GPS based velocity measurements for measurement of sideslip and wheel slip', *Vehicle System Dynamics*, Vol. 38, No. 2, pp.127–147.

Bevly, D.M., Daily, R. and Travis, W. (2006) *Estimation of Critical Tire Parameters using GPS Based Sideslip Measurements*, SAE Paper 2006-01-1965.

Brogan, W.L. (1991) *Modern Control Theory*, Upper Saddle River, Prentice-Hall Inc., NJ, ISBN: 0-13-589763-7.

Daily, R. and Bevly, D.M. (2004) 'The use of GPS for vehicle stability control systems', *IEEE Transactions on Industrial Electronics*, Vol. 51, No. 2, pp.270–277.

Dugoff, H., Fancher, P.S. and Segel, L. (1970) *An Analysis of Tire Traction Properties and their Influence on Vehicle Dynamic Performance*, SAE Paper 700377, pp.1219–1243.

Farrelly, J. and Wellstead, P. (1996) 'Estimation of vehicle lateral velocity', *Proceedings from the 1996 IEEE Conference on Control Application*, pp.552–557.

Gebre-Egziabher, D. (2004) *Design and Performance Analysis of a Low Cost Aided Dead Reckoning Navigator*, Thesis (PhD), Stanford University, Department of Aeronautics and Astronautics, Palo Alto, California.

Gillespie, T.D. (1992) *Fundamentals of Vehicle Dynamics*, Society of Automotive Engineers, ISBN: 1-56091-199-9, Warrendale, Pa.

Hac, A. and Simpson, M. (2000) *Estimation of Vehicle Side Slip Angle and Yaw Rate*, SAE Paper 2000-01-0696.

Hahn, J. and Rajamani, R. (2002) 'GPS-based real-time identification of tire-road friction coefficient', *IEEE Transactions on Control Systems Technology*, Vol. 10, No. 3, pp.331–343.

Heydinger, G.J., Bixel, R.A., Garrott, W.R., Pyne, M., Howe, J.G. and Guenther, D.A. (1999) *Measured Vehicle Inertial Parameters – NHTSA's Data through November 1998*, SAE Paper 1999-01-1336.

Hong, S., Choi, J.U. and Speyer, J.L. (2001) 'Estimation of errors in INS with multiple GPS antennas', *Proceeding from the 2001 IEEE Conference on Industrial Electronic Conference*, Vol. 1, pp.410–415.

Hsu, Y.J. and Gerdes, J.C. (2005) 'Stabilization of a steer-by-wire vehicle at the limits of handling using feedback linearization', *Proceedings of IMECE 2005*.

Koo, S., Tan, H. and Tomizuka, M. (2004) 'Nonlinear tire lateral force versus slip angle curve identification', *Proceedings of the American Control Conference 2004*, Vol. 3, pp.2128–2133.

Kwak, B., Park, Y. and Kim, D. (2000) 'Design of observer for vehicle stability control system', *Proceedings of the FISITA 2000 World Automotive Congress*.

M'Sirdi, N.K., Rabhi, A., Zbiri, N. and Delanne, Y. (2005) 'Vehicle-road interaction modeling for estimation of contact forces', *Vehicle System Dynamics*, Vol. 43, pp.403–411.

Müller, S., Uchanski, M. and Hedrick, K. (2003) 'Estimation of the maximum tire-road friction coefficient', *Journal of Dynamic Systems, Measurement, and Control*, Vol. 125, pp.607–617.

Nishio, A., Tozu, K., Yamaguchi, H., Asano, K. and Amano, Y. (2001) *Development of Vehicle Stability Control Based on Vehicle Sideslip Angle Estimations*, SAE Paper No. 2001-01-0137.

O'Brien, R. and Kiriakidis, K. (2006) 'A comparison of H_∞ with Kalman filtering in vehicle state and parameter identification', *Proceedings of the American Control Conference 2006*, pp.3954–3959.

Ray, L. (1995) 'Nonlinear state and tire force estimation for advanced vehicle control', *IEEE Transaction on Control System Technology*, Vol. 3, No. 1, pp.117–124.

Rock, K.L., Beiker, S.A., Laws, S. and Gerdes, J.C. (2005) 'Validating GPS based measurements for vehicle control', *Proceedings of IMECE 2005*.

Ryu, J., Rossetter, E.J. and Gerdes, J.C. (2002) 'Vehicle sideslip and roll parameter estimation using GPS', *Proceeding of the AVEC 2002*, pp.373–380.

St. Pierre, M. and Gingras, D. (2004) 'Comparison between the unscented Kalman filter and the extended Kalman filter for the position estimation module of an integrated navigation information system', *IEEE Symposium on Intelligent Vehicles 2004*, Parma, Italy.

Stengal, R. (1994) *Optimal Control and Estimation*, Dover Publications, Mineola, NY, ISBN: 0-486-68200-5.

Switkes, J.P. and Gerdes, J.C. (2005) 'Guaranteed lanekeeping performance with tire saturation using computed polynomial Lyapunov functions', *Proceedings of IMECE 2005*.

Titterton, D.H. and Weston, J.L. (1997) *Strapdown Inertial Navigation Technology*, Peter Peregrinus, London, England.

Travis, W. and Bevly, D.M. (2005) 'Navigation errors introduced by ground vehicle dynamics'. *Proceedings of the ION GNSS 2005*, pp.302–310.

Tseng, H.E., Madau, D., Ashrafi, B., Brown, T. and Recker, D. (1999) 'Technical challenges in the development of vehicle stability control system', *Proceeding from the 1999 IEEE International Control Conference on Control Applications*, Vol. 2, pp.1660–1666.

van Zanten, A.T. (2002) 'Evolution of electronic control systems for improving the vehicle dynamic behavior', *Proceedings of the 2002 AVEC*, pp.7–15.

Nomenclature

m	Vehicle mass
I_z	Vehicle yaw moment of inertia
L	Vehicle wheel base
a	Distance from the front axle to the vehicle CG
b	Distance from the rear axle to the vehicle CG
$C_{\alpha f,\alpha r}$	Front and rear tire cornering stiffnesses
K_{US}	Vehicle understeer gradient
μ	Peak tire coefficient of friction
F_z	Vertical load on tire
θ	Vehicle roll angle

δ	Vehicle steer angle
r	Vehicle yaw rate
a_y	Vehicle lateral acceleration
ψ	Orientation of the vehicle centreline (vehicle heading)
ν	Horizontal velocity vector orientation (vehicle course)
$V_{x,y}$	Longitudinal and lateral velocity
β	Vehicle sideslip angle at the CG
$\alpha_{f,r}$	Front and rear tire slip angles
b_{gyro}	Yaw rate gyro bias
b_{accel}	Lateral accelerometer bias